Proceedings of the 20th International Conference on Soil Mechanics and Geotechnical Engineering– Rahman and Jaksa (Eds)

Large deformation finite-element modeling of pile jacking in sensitive clay

Modélisation par éléments finis de grandes déformations du fonçage de pieux dans l'argile sensible

Ripon Karmaker & Bipul Hawlader
Memorial University of Newfoundland, St. John's, NL, Canada, rkarmaker@mun.ca

ABSTRACT: This study presents Coupled Eulerian-Lagrangian (CEL) finite element (FE) analyses of pile jacking in sensitive clays. Implementing the effects of strain rate and strain softening on undrained shear strength of sensitive clay, the process is simulated over a large penetration distance for varying sensitivities and rate of shear strength degradation with plastic shear strain. The simulation results show that the soil flow mechanisms and development of plastic shear strains in the soil around the pile are significantly influenced by the sensitivity; therefore, the modelling with idealized soil conditions (i.e., without strain-rate and softening effects) cannot simulate the installation process properly for highly sensitive clays. For high sensitivity, large plastic shear strains develop in a narrow zone near the pile, which could reduce the shaft friction to a very low value; however, the plastic shear strains distributed over a larger area for the soil of lower sensitivity and a lower rate of shear strength degradation.

RÉSUMÉ : Cette étude présente des analyses par éléments finis (EF) couplés eulérien-lagrangien (CEL) du fonçage de pieux dans des argiles sensibles. En mettant en œuvre les effets de la vitesse de déformation et de l'adoucissement de la déformation sur la résistance au cisaillement non drainée de l'argile sensible, le processus est simulé sur une grande distance de pénétration pour différentes sensibilités et taux de dégradation de la résistance au cisaillement avec la déformation de cisaillement plastique. Les résultats de la simulation montrent que les mécanismes d'écoulement du sol et le développement des déformations plastiques de cisaillement dans le sol autour du pieu sont significativement influencés par la sensibilité ; par conséquent, la modélisation avec des conditions de sol idéalisées (c'est-à-dire sans effets de vitesse de déformation et de ramollissement) ne peut pas simuler correctement le processus d'installation pour les argiles très sensibles. Pour une sensibilité élevée, de grandes déformations de cisaillement plastique se développent dans une zone étroite près du pieu, ce qui pourrait réduire le frottement de l'arbre à une valeur très faible ; cependant, les déformations de cisaillement plastique se sont réparties sur une plus grande surface pour le sol de sensibilité inférieure et un taux de dégradation de la résistance au cisaillement plus faible.

KEYWORDS: pile jacking; large deformation; finite element analysis; sensitive clay.

1 INTRODUCTION

Pile jacking is one of the pile installation processes that create less ground vibration and disturbances than traditional pile installation methods. This method of pile installation has gained popularity in urban environments to avoid/reduce disturbance on pre-existing infrastructures due to pile installation (White et al. 2002). However, pile jacking causes a large volume of soil displacements, and the displaced soils predominantly cause ground heave during the shallow depth of penetration and local radial displacement for the higher depth of penetration. Several theoretical (Baligh 1976, Sagaseta 1987, Teh & Houlsby 1991, Sagaseta & Whittle 2001), experimental (Flaate 1972, Bozozuk et al. 1978, Blanchet et al. 1980, Roy et al. 1981) and numerical (Qui et al. 2011, Tian et al. 2011, Tho et al. 2012, Karmaker et al. 2019, Zhou et al. 2019) investigations were carried out to find the ground responses during and after pile installation.

The installation of piles in sensitivity clay shows some unique features. For example, Roy et al. (1981) presented the results of a field test program where six instrumented piles of 219-mm diameter (D) were jacked into a highly sensitive clay layer. During continuous penetration (e.g., #5 of their study), no significant increase in shaft friction contribution to the total load was found. This implies that the shaft friction of sensitive clay may not be significant during continuous penetration. They also conducted vane shear tests around the pile before and after pile installation and showed that the installation reduced the undrained shear strength up to ~3D from the pile surface. The disturbance of soil is high near the pile, although the strength could not be measured very close to the pile surface, which governs the shaft friction. Azzouz & Morrison (1988) presented field test results from two sites where the soils were lightly overconsolidated (OCR = 1.2–1.5) but different sensitivities: (a) Lower Boston Blue Clay ($S_t = 7 \pm 2$), and (b) Lower Empire Clay ($S_t = 2 \pm 1$). They used piezo-lateral stress cells for continuous measurement of total horizontal stress and pore water pressure. A very different response was observed during pile installation: the effective horizontal stress near the pile surface is almost zero for sensitive Boston Blue Clay while it is considerably high for the low sensitive Lower Empire Clay. This again implies that the remoulding of soil during penetration increases with the sensitivity that might have increased the pore water pressure. Unfortunately, the remoulding process cannot be measured directly in the field. Therefore, numerical simulations might provide some further insights.

Pile jacking is a large deformation process, which cannot be simulated using typical Lagrangian-based FE modelling techniques. The authors of the present study developed CEL models to analyze the installation of piles in clay and sand considering idealized soil behaviour (Karmaker et al. 2019). The main objective of this study is to present the simulations of pile jacking in sensitive clay to investigate the effects of strain rate and strain softening on penetration resistance and soil disturbance.

2 PROBLEM STATEMENT

A solid pile of 0.4-m diameter is penetrated in a sensitive clay layer at a constant velocity along the z-axis, as shown in Fig. 1. The position of the pile tip at a given instant, measured from the ground surface prior to installation, is w_{tip}. The penetration is continued up to 10 pile diameter. In the beginning, the pile tip is kept slightly above the ground level to avoid any interaction between pile and soil during the application of gravity load, as discussed in the following sections.

The analysis is performed for an undrained condition. A linearly increasing initial undrained shear strength (s_{u0}) profile is considered.

$$s_{u0} = s_{ug} + kz \quad (1)$$

Where s_{u0} is the initial undrained shear strength before any

softening and at the reference strain rate, as discussed below; s_{ug} is the shear strength at the ground surface in kPa; k is the strength gradient in kPa/m, and z is the depth of soil element below the ground surface in meters. The groundwater table is considered at the ground surface. The pile is considered a rigid body.

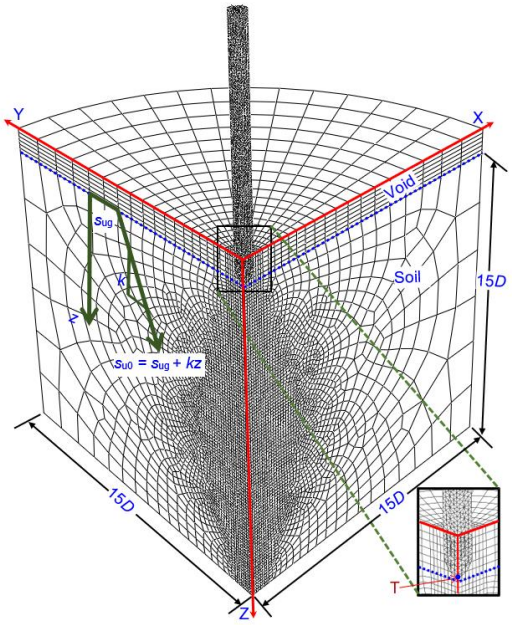

Figure 1. Finite element mesh used in analysis

3 FINITE ELEMENT MODELING

The Coupled Eulerian-Lagrangian (CEL) approach available in Abaqus 2019 is used. The CEL can model large deformation problems without any numerical issues related to mesh distortion. The simulation process can be viewed as the flowing of soil, as an Eulerian material, through a fixed mesh.

Taking the advantages of symmetry, only a quarter of the whole domain is modelled. A dense mesh is used in the zone around the pile where significant deformation of soil is expected. A cylindrical boundary is placed at a radial distance of 15D from the pile center. The total height of the soil model is 15D. Analyses are also performed with a larger soil domain than that described above; however, no significant change in the result is found.

The soil and the pile are modelled as an Eulerian material and Lagrangian rigid body, respectively. The model has three parts: soil, pile, and void. The soil and void are defined using the Eulerian Volume Fraction (EVF) tool available in the software, where EVF = 1 means the element is filled with soil and EVF = 0 means no soil in the element (void). During the analysis, some elements might be partially filled with soil (0 < EVF < 1). The soil elements are modelled using the EC3D8R element in the software, which are linear multi-material Eulerian brick elements. The clay is modelled as an elastic-perfectly plastic material using the von Mises yield criteria incorporating strain-softening and the strain-rate effects, as discussed later. Zero-velocity boundary conditions are used normal to all the vertical faces. In the curved cylindrical outer surface, the soil is allowed to move only in the vertical direction. At the bottom of the domain, zero-velocity boundary conditions are applied in all three directions (i.e. $v_x = v_y = v_z = 0$), meaning that the soil elements next to this boundary are restrained from any movement. No boundary condition is applied at the soil–void interface so that the soil can displace into the void during the penetration of the pile when needed (e.g., ground surface heaving near the pile). The parameters used in the analysis are listed in Table 1. A detailed discussion on the selection of the soil parameters is available in Dey et al. (2015, 2016) and Wang et al. (2020).

The pile–soil interface is modelled as a frictional contact using the default general contact formulation in the software. In the present undrained total stress analysis, the Coulomb friction law is implemented by limiting the maximum shear stress at the soil–pile interface (τ_{max}) to αs_{u0}, where $0 \le \alpha \le 1.0$. Previous studies also suggested that α could be estimated as the inverse of the sensitivity (Einav & Randolph 2005, Hossain & Randolph 2009). A large value of Coulomb friction coefficient (= 50) is taken to ensure quick mobilization of τ_{max}. Although s_{u0} increases with depth, a constant value of τ_{max} is used.

Table 1: Geotechnical properties used in EF analysis

Parameters	Value
Total unit weight, γ (kN/m^3)	17
Undrained Young's modulus, E_u (MPa)	10
Undrained Poison's ratio, ν_u	0.49
Shear strength at the ground surface, $s_{u,g}$ (kPa)	20
Strength gradient, k (kPa/m)	1.67
Reference shear strain rate, $\dot{\gamma}_{ref}$	5.0
Viscous property, η	0.5
Shear-thinning index, β	0.1
δ_{95_u} (m)	0.1, 0.4
S_t (= s_{u0}/s_{uR})	2, 5, 10, 20

The FE analysis consists of two steps of loading. First, gravity is applied to the soil to bring it to the *in-situ* stress condition. Using a predefined field, the expected geostatic stress distribution is assigned first to the soil elements, and then the gravity load is applied using body force. Predefined stresses reduce excessive deformation of soil during gravity loading. Earth pressure coefficient of 0.96 is used. Note that the earth pressure coefficient at rest for Canadian sensitive clays is significantly higher than that obtained from Jaky's formula and is also higher than many Norwegian sensitive clays. A detailed discussion is available in previous studies (Hamouche et al. 1995, L'Heureux et al. 1917, Wang et al. 2020).

In the second step, the pile is penetrated at a constant velocity of 0.1 m/s. Several field investigations were carried out at jacking velocity of 0.01–0.001 m/s (e.g., Roy et al. 1981, Yang et al. 2006, Kou et al. 2015), which are 10 to 100 times slower than the adopted velocity in the present study. In numerical analysis, such a slow rate of penetration is not required because it unnecessarily increases the computational time (Tho et al. 2006, Wang et al. 2015). Rather the simulations should be performed maintaining the quasi-static condition, which generally occurs if the kinetic energy of the model does not exceed 5%–10% of its internal energy and the external work done is nearly equal to the internal energy throughout the analysis (Robert et al. 2020).

3.1 *Strain-softening and strain-rate effects*

The mobilized undrained shear strength (s_u) of sensitive clay is modelled using Eq. (2), incorporating a strain-softening factor, f_1 (≤ 1.0), and strain-rate factor, f_2.

$$s_u = f_1 f_2 s_{uy} \tag{2}$$

Where, s_{uy} is the undrained shear strength at a very low strain rate. Linear and exponential functions have been used in previous studies to define the reduction of shear strength as a function of accumulated plastic shear strain (ξ) or plastic shear displacement (δ) (Locat et al. 2013, Dey et al. 2015, Wang et al. 2020). In the present study, the following equations are used to define the post-peak degradation undrained shear strength (Dey et al. 2016, Wang et al. 2020):

$$f_1 = \begin{cases} \frac{s_{uR}}{s_{u0}} + \left(1 - \frac{s_{uR}}{s_{u0}}\right) e^{-3\delta/\delta_{95}} & \text{if } 0 \le \delta < 2\delta_{95} \\ \frac{s_{uR}}{s_{u0}} - \frac{s_{uR} - s_{uld}}{s_{u0}} \frac{\delta - 2\delta_{95}}{\delta_{ld} - 2\delta_{95}} + c & \text{if } 2\delta_{95} \le \delta < \delta_{ld} \\ \frac{s_{uld}}{s_{u0}} + c & \text{if } \delta \ge \delta_{ld} \end{cases} \quad (3)$$

where s_{u0} is the peak undrained shear strength at the reference shear strain rate ($\dot{\gamma}_{ref}$) before softening; s_{uR} is the value of s_u at sufficiently large δ; δ_{95} is the value of δ at which 95% reduction of (s_{u0} - s_{uR}) occurs; $c = (1 - s_{uR}/s_{u0})e^{-6} \approx 0$; and δ_{ld} is a very large value of δ (> δ_{95}) when the soil becomes completely remoulded to $s_u = s_{uld}$. The rate of post-peak shear strength degradation primarily depends on S_t and δ_{95}. Further details on the above strain-softening equations, including the selection of the model parameters, are available in Dey et al. (2015) and Wang et al. (2020).

For strain-softening materials, the solution is generally mesh-size dependent. Various mesh regularization techniques have been proposed in the past to reduce mesh dependency, as discussed in previous studies (e.g., Gylland 2012). For a given δ in Eq. (3), the finer mesh in Fig. 1 would give higher shear strain. In the present study, an element size scaling rule, similar to that presented in Dey et al. (2015), is used. Table 1 shows the value of δ_{95_u} for a unit shear band thickness. The value of δ_{95} of a soil element is calculated as δ_{95_u}/t_{FE} where t_{FE} represents the size of the element. In this study, the characteristic length is used as t_{FE}. In the subroutine, t_{FE} is called, which is then used to calculate the element-size dependent δ_{95}, which is then used to calculate the post-peak strength degradation factor f_1 using Eq. (3).

For strain-rate effects, a geotechnical approach could be used for low strain levels; however, a fluid mechanics approach would be more appropriate for the remoulded condition. An "additive power-law model" proposed by Zhu & Randolph (2011), which combines the Herschel-Bulkley (fluid mechanics approach) and power-law model (geotechnical approach), is used in this study:

$$f_2 = \left[1 + \eta\left(\dot{\gamma}/\dot{\gamma}_{ref}\right)^{\beta}\right] \quad (4)$$

where η and β are the soil parameters. The value of η depends on the reference shear strain rate. The typical range of β is 0.05–0.15, which increases with the plasticity index. The selection of these soil parameters has been discussed in Randolph et al. (2012) in general and Wang et al. (2020) for sensitive clays. Using $\dot{\gamma} = \dot{\gamma}_{ref}$ in Eq. (4) and then inserting f_2 in Eq. (2) with $f_1 = 1.0$ (no softening) and $s_u = s_{u0}$, the undrained shear strength at a very low strain rate can be calculated as $s_{uy} = s_{u0}/(1 + \eta)$. However, in the field, the process becomes partially drained or drained at a low rate of shearing. For example, vane shear tests in low plastic sensitive clays show that the shear strength does not decrease at a very slow rate of rotations rather increases because of excess pore water pressure dissipation (Roy & Leblanc 1988). Therefore, in the present study, $s_u = s_{u0}$ is used when $\dot{\gamma} \le \dot{\gamma}_{ref}$. Also, as the numerical simulation is performed with a higher penetration rate than the typical field jacking rate (discussed above), a higher value of $\dot{\gamma}_{ref}$ is used to model comparable rate effects on s_u.

User subroutines are used to implement the variation of s_u with depth and the effects of strain rate and strain-softening. Further details are available in Dutta et al. (2015) and Wang et al. (2020).

4 RESULTS

In the following sections, the discussion is mainly focused on force-displacement behaviour and the development of plastic shear strains around the pile. The latter one has a profound effect on the disturbance of sensitive clay and subsequent load-carrying capacity.

The reaction force at the reference point of the rigid pile in FE analysis gives the total penetration resistance (F) at a given pile tip depth (w_{tip}). Subtracting the buoyancy contribution (F_b), as discussed in Karmaker et al. (2019), the normalized penetration resistance (N) is calculated as $N = (F - F_b)/\left(\frac{2}{\sqrt{3}} s_{u0} A_p\right)$, where A_p is the cross-sectional area of the pile tip (see Hawlader et al. 2016 for further details on normalization). The equivalent plastic shear strain, ε_q^p (PEEQVAVG in the software), is used to define the plastic zone and soil disturbance.

4.1 *Effects of pile–soil interface resistance*

Pile–soil interface resistance for sensitive clays might vary significantly, depending upon the degree of remoulding and pore pressure generation (e.g., Azzouz & Morrison 1988). The parameter δ_{95} in Eq. (3) is related to the rate of remoulding —the lower the value of δ_{95} the faster the remoulding. To investigate the effects of skin friction, analyses are performed for five interface conditions: smooth, τ_{max} = 6 kPa, τ_{max} = 10 kPa, τ_{max} = 15 kPa and rough. One more analysis is performed for the smooth condition without considering the effects of softening and strain rate (ideal soil, where $f_1 = f_2 = 1$).

Figure 2(a) shows that, for the smooth condition, the penetration resistance (N) is higher for the ideal soil than that with strain-rate and strain-softening (δ_{95_u} = 0.1 m) effects. This implies that the mobilized s_u (Eq. (2)) is smaller than s_{u0} of the ideal soil. A similar analysis for the smooth condition but with δ_{95_u} = 0.4 m also gives smaller N than that of the ideal soil; however, the difference is smaller than that shown in Fig. 2(a). These two sets of analyses show that strain-softening could have a significant effect on the penetration resistance of a pile in highly sensitive clays.

For the ideal soil case, N increases with the depth of penetration; however, the rate of increase of N decreases at larger depths. The value of N is 10.5 at w_{tip}/D = 9.5. Teh & Houlsby (1991) showed that the normalized cone penetration resistance also depends on the rigidity index, I_r (=G/s_u). For a smooth interface condition and uniform s_u profile, they found $N \sim 10$ and $N \sim 13$ for I_r = 100 and I_r = 300, respectively. In the present study, I_r = 167 and s_{u0} increases with depth. Also, based on theoretical modelling, Meyerhof (1951) calculated N = 9.34 for deep circular foundations.

Figures 2(a) and 2(b) show that the rate of penetration resistance increase with depth increases with τ_{max}. The rough interface condition gives a rapid increase in N at a shallower depth; however, at larger depths, the N increases slowly. Below w_{tip}/D = 8, the calculated N for τ_{max} = 15 kPa is similar to that of the rough condition.

4.2 *Effects of sensitivity*

Figure 3 shows the effects of sensitivity, S_t (= s_{u0}/s_{uR}), on penetration resistance for two values of δ_{95_u} (= 0.1 & 0.4 m) and smooth interface condition. For δ_{95_u} = 0.1 m, N decreases significantly with an increase in S_t (Fig. 3(a))—for example, at w_{tip}/D = 9.5, N is ~8.8 and ~5.8 for S_t = 2 and S_t = 20, respectively. For δ_{95_u} = 0.4 m, no significant difference in N is observed for S_t = 5 to 20 because of the slower rate of remoulding. Note that, for idealized weightless soil with uniform undrained shear strength, the N becomes constant after ~8D penetration for smooth pile–soil interface condition, as discussed in Karmaker et al. (2019).

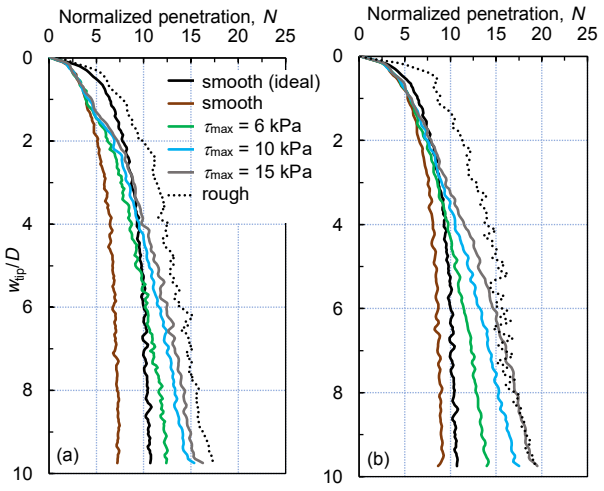

Figure 2. Effects of shaft friction on penetration resistance: (*a*) δ_{95_u} = 0.1 m, (*b*) δ_{95_u} = 0.4 m

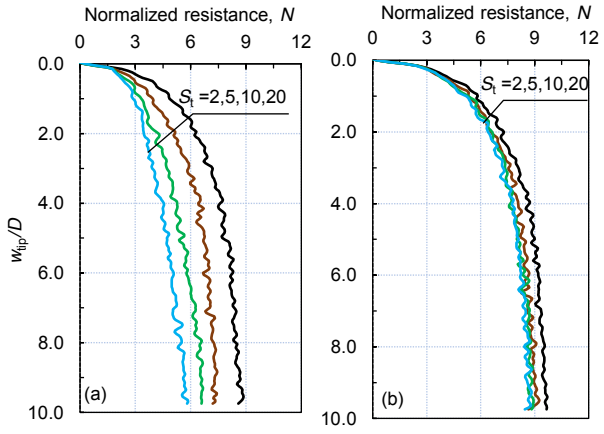

Figure 3. Effects of sensitivity on penetration resistance: (*a*) δ_{95_u} = 0.1 m, (*b*) δ_{95_u} = 0.4 m

4.3 *Reduction of undrained shear strength around piles*

When a pile is jacked into the sensitive clay, the disturbance could reduce the undrained shear strength of soil within a radial distance of several pile diameters. Figure 4 shows the mobilized s_u normalized by s_u far from the pile at the same depth. The results are shown for six different radial distances (r) measured from the centerline of the pile and at 4 m penetration depth. The mobilized s_u is small near the pile, and it increases with radial distance. One interesting observation is that, for a given radial distance of 0.875D–2.0D, the mobilized s_u is higher near the ground surface (e.g., z < 2 m for r = 0.825D) and then decreases to smaller values at larger depth. When the pile tip is at a shallower depth (z < 2 m), the soil can move outward because of the free boundary at the ground surface. However, when the pile tip moves sufficiently deep, the displaced soil around the pile tip tries to move through the weak remoulded soil near the pile, which increases the plastic shear strains and causes further reduction of mobilized shear strength. This type of soil movement does not occur in non-sensitive clays. Significant remoulding of soil near the pile and possible pore pressure generation could mobilize a very small shaft friction during installation, as observed in field tests (e.g., Roy et al. 1981)

Figure 4 shows that, with an increase in radial distance, the mobilized s_u increases, which means less remoulding of soil at a larger distance. Almost no reduction of s_u occurs in the soil elements at a radial distance larger than 4.0D. The maximum reduction of strength is ~80% for r = 0.625D while it is ~10% for r = 2.0D. This indicates that a highly remoulded zone formed within ~2 pile diameters. Based on field test results, some studies showed a similar extend of disturbed zone (Flaate 1972, Bozozuk et al. 1978).

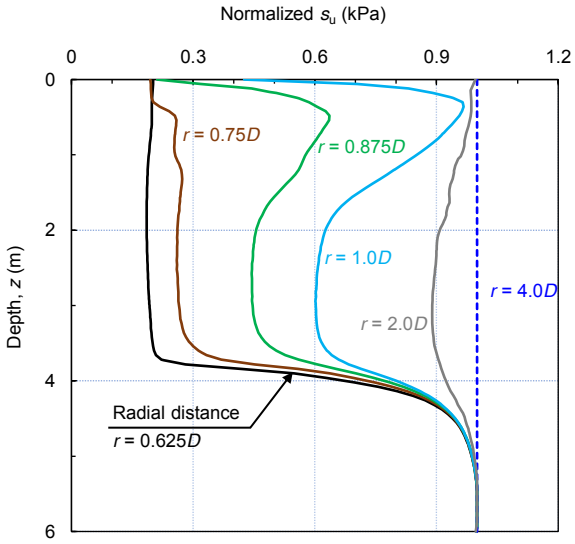

Figure 4. Mobilized undrained shear strength at different radial distances from pile center for 4-m penetration depth

4.4 *Effects of strain rate and softening*

Equation (2) shows that the mobilized s_u depends on strain softening (f_1) and strain rate (f_2). The mobilized s_u finally governs the penetration resistance and soil flow mechanisms. Figure 5 shows the contours of f_1 when the pile is penetrated to 4 m depth. The results are shown for four different sensitivities (S_t = 2, 5, 10 & 20). In these analyses, smooth interface condition and δ_{95_u} = 0.1 m are used. The other parameters are the same as Table 1. Very different strength softening zones are found depending upon sensitivity. The strength degradation occurs over a larger area for low S_t. For high sensitivity (S_t = 20.0), the soil in a narrow zone around the pile becomes completely remoulded and flows up like a fluid.

As a high value of reference shear strain rate is used, the rate effect is not significant for the penetration rate considered in this study.

To explain the mechanisms further, the development of plastic shear strains in the soil around the pile when it is penetrated to 4.0 m depth is shown in Fig. 6. Analyses are performed for three different sensitivities (S_t = 2, 5, 10), again with δ_{95_u} = 0.1 m and δ_{95_u} = 0.4 m. Figure 6(a) shows that, for low sensitivity (S_t = 2), the plastic shear strains distribute over a large area. On the other hand, the plastic shear strains accumulated in a narrower zone for higher sensitivity (e.g., Fig. 6(c)). Moreover, in the highly sensitive clay, large plastic shear strains develop near the pile (Fig. 6(c)), as compared to those in the low sensitive clay (Fig. 6(a)). Recall that strength degradation depends on plastic shear strain (Eq. (3)). Therefore, the shaft friction in highly sensitive clays is expected to be less than that of low sensitive clays.

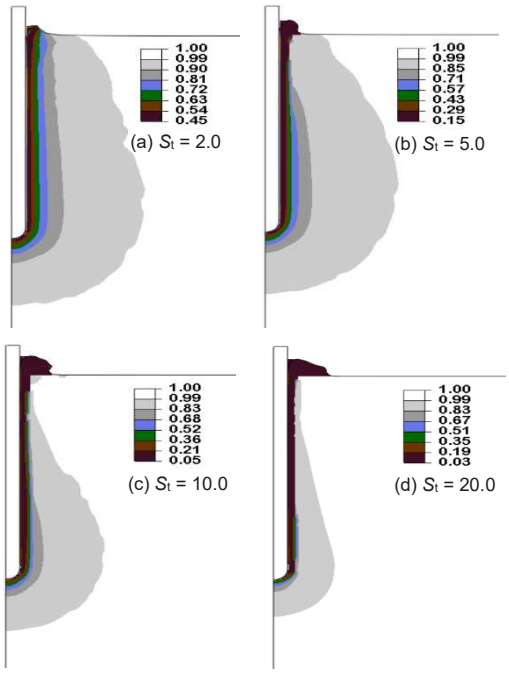

Figure 5. Strain-softening effects on soil deformation for 4-m penetration depth

5 CONCLUSIONS

Analytical methods (e.g., cavity expansion and strain path methods) are available to model the response of soil around the pile during installation. Numerical studies are also available, primarily for idealized soil conditions. The present study examines the effects of pile installation in sensitive clays. Large deformation finite element analyses are performed incorporating the effects of strain rate and strain softening on undrained shear strength.

The disturbance of soil around the pile is significantly influenced by the sensitivity of the soil and the rate of remoulding. The size of the plastic zone around the pile is smaller for higher sensitive clays. However, the magnitude of plastic shear strain is higher in high sensitive clays. More importantly, a narrow zone near the pile surface might be significantly remoulded due to the development of high plastic shear strains that could reduce the pile–soil interface resistance to a very low value, as observed in some field tests where the contributions of shaft friction to the total penetration resistance do not increase with penetration in sensitive clays. A slower rate of post-peak softening with plastic shear strain does not degrade the shear strength significantly and shows less effect on penetration resistance. In summary, the rate of shear strength degradation, which is a combined effect of S_t and δ_{95_u}, is a key factor that changes the response during penetration of a pile in sensitive clays.

6 ACKNOWLEDGEMENTS

The work presented in this paper has been supported by the Natural Sciences and Engineering Research Council of Canada (NSERC), Equinor, Petroleum Research Newfoundland and Labrador and Mitacs.

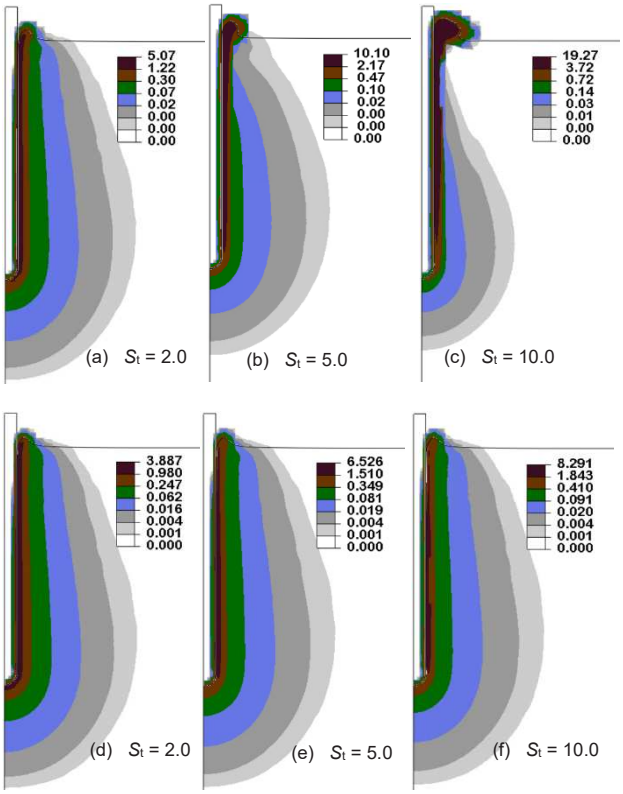

Figure 6. Plastic shear strains for different sensitivities for 4 m pile penetration depth: (*a*)–(c) δ_{95_u} = 0.1 m, (d)–(f) δ_{95_u} = 0.4 m

7 REFERENCES

Azzouz A.S. and Morrison M. 1988. Field measurements on model pile in two clay deposits. *J. Geot. Eng*, 114(1), 104–121.

Baligh M.M. 1976. Cavity expansion in sand with curved envelopes. *J. Geot. Eng. Div.,* 102(11), 1131–1146.

Blanchet R., Tavenas F. and Garneau R. 1980. Behaviour of friction piles in soft sensitive clay. *Can. Geotech. J.*, 17(2), 203–224.

Bozozuk M., Fellenius B.H. and Samson L. 1978. Soil disturbance from pile driving in sensitive clay. *Can. Geotech. J*., 15, 346–361.

Dey R., Hawlader B., Phillips R. and Soga K. 2015. Large deformation finite-element modeling of progressive failure leading to spread in sensitive clay slopes. *Géotechnique,* 65(8), 657–668.

Dey R., Hawlader B., Phillips R., and Soga K. 2016. Modeling of large-deformation behaviour of marine sensitive clays and its application to submarine slope stability analysis. *Can. Geotech. J.*, 53(7), 1138–1155.

Dutta S., Hawlader B., and Phillips R. 2015. Finite element modeling of partially embedded pipelines in clay seabed using Coupled Eulerian-Lagrangian method. *Can. Geotech. J.*, 52, 52–72.

Einav I. and Randolph M.F. 2005. Combining upper bound and strain path methods for evaluating penetration resistance. *Int. J. Num. Meth. Eng.*, 63(14), 1991–2016.

Flaate K. 1972. Effects of pile driving in clays. *Can. Geotech. J*., 9, 81–88.

Gylland A.S. 2012. Material and slope failure in sensitive clays. *Ph.D. thesis*. Norwegian University of Science and Technology.

Hamouche K.K., Leroueil S., Roy M., and Lutenegger A. J. 1995. In situ evaluation of K0 in eastern Canada clays. *Can. Geotech. J*., 32(4), 677–688.

Hawlader, B., Fouzder, A., and Dutta, S. 2016. Numerical modeling of suction and trench formation at the touchdown zone of steel catenary riser. *Int. J. Geomech.*, 16 (1), 04015033.

Hossain M.S. and Randolph M.F. 2009. Effect of strain rate and strain softening on the penetration resistance of spudcan foundations on clay. *Int. J. Geomech.*, 9, 122–132.

Karmaker R., Hawlader B., and Chen W. 2019. Finite element modeling of jacked piles in clay and loose sand. *72nd Can. Geotech. Conf., GeoSt.John's 2019,* St. John's, NL, Canada. Paper No-436.

Kou H., Zhang M. and Yu F. 2015 Shear zone around jacked piles in clay, *J. Perform. Const. Facilities.*, 29(6), 04014169.

L'Heureux J. S., Ozkul Z., Lacasse S., D'Ignazio M. and Lunne T. 2017. A revised look at the coefficient of earth pressure at rest for Norwegian clays. *In Fjellsprengningsteknikk, Bergmekanikk/ Geoteknikk (eds K. K. Dunham, Ø. Dammyr, M. Rømoen and S. Engen)*, 35.1-35.11.

Locat A., Jostad H.P. and Leroueil S. 2013. Numerical modeling of progressive failure and its implications for spreads in sensitive clays. *Can. Geotech. J.*, 50(9), 961–978.

Meyerhof G. G. 1951. The ultimate bearing capacity of foundations. *Géotechnique*, 2(4), 301–332.

Qiu G., Henke S. and Grabe J. 2011. Application of a Coupled Eulerian–Lagrangian approach on geomechanical problems involving large deformations. *Comp. and Geotech.,* 38, 30–39.

Randolph M.F., White D.J. and Yan Y. 2012. Modelling the axial soil resistance on deep-water pipelines. *Géotechnique*, 62(9), 837-846.

Robert D.J., Britto A. and Setunge S. 2020. Efficient approach to simulate soil-pipeline interaction. *J. Pipeline. Syst. Eng. Pract*., 11(1), 04019046.

Roy M. and Leblanc A. 1988. Factors affecting the measurements and interpretation of the vane strength in soft sensitive clays, *Vane shear strength testing in soils: field and laboratory studies*, ed. A. Richards, West Conshohocken, PA, 117–128.

Roy M., Blanchet R., Tavenas F. and Rochelle P.L. 1981. Behaviour of a sensitive clay during pile driving. *Can. Geotech. J*., 18(1), 67–85.

Sagaseta C. 1987. Analysis of undrained soil deformation due to ground loss. *Géotechnique*, 37(3), 301–320.

Sagaseta C. and Whittle J. 2001. Prediction of ground movements due to pile driving in clay. *J. Geotech. Geoenviron. Eng*., 127(1), 55–66.

Teh C.I. and Houlsby G.T. 1991. An analytical study of the cone penetration test in clay. *Géotechnique*, 41(1), 17–34.

Tho K.K., Leung C.F., Chow Y.K., and Swaddiwudhipong S. 2012. Eulerian finite-element technique for analysis of jack up spudcan penetration. *Int. J. Geomech*., 12(1), 64–73.

Tian Y., Wang D. and Cassidy M. 2011. Large deformation finite element analysis of offshore geotechnical penetration tests. *Proc.2nd Int. Symp. Comp. Geomech., USA*, 1, 925-933.

Wang C., Hawlader B., Perret D. and Soga K. 2020. Effects of geometry and soil properties on type and retrogression of landslides in sensitive clays. *Géotechnique*, doi.org/10.1680/jgeot.20.P.046.

Wang D., Bienen B., Nazem M., Tian Y., Zheng J., Pucker T. and Randolph M. F. 2015. Large deformation finite element analysis in geotechnical engineering. *Comp. and Geotech.*, 65, 104–114.

White D., Finlay T., Bolton M., and Bearss G. 2002. Press-in piling: ground vibration and noise during pile installation. *Deep Foundations 2002*, 363–371.

Yang J., Tham L.G., Lee P.K., Chan S. T. and Yu F. 2006. Behaviour of jacked and driven piles in sandy soil. *Géotechnique*, 56(4), 245–259.

Zhou H., Liu H., Yuan J. and Chu J. 2019. Numerical simulation of XCC pile penetration in undrained clay. *Comp. and Geotech.*, 106, 18–41.

Zhu H. and Randolph M.F. 2011. Numerical analysis of a cylinder moving through rate dependent undrained soil. *Ocean Eng.* 38(7), 943–953.